Int. J. Heat Mass Transfer. Vol. 36, No. 14, pp. 3487–3496, 1993
Printed in Great Britain

0017-9310/93 $6.00+0.00

Local heating induced by a nonhomogeneously distributed heat source

DA YU TZOU and JING LI
Department of Mechanical Engineering, University of New Mexico, Albuquerque, NM 87131, U.S.A.

(*Received* 17 *September* 1992 *and in final form* 2 *February* 1993)

Abstract—The thermal wave behavior in the vicinity of a fast-moving heat source is studied in this work. The heating zone is modelled by a circular region with a finite radius and the intensity of the heat-production rate is assumed to be nonhomogeneously distributed. The Green's functions obtained previously by Tzou [*ASME J. Heat Transfer* **111**, 232–238 (1989); *Int. J. Heat Mass Transfer* **32**, 1979–1987 (1989)] are used to integrate the temperature waves emanating from the heating zone. A complete description covering the subsonic, transonic and supersonic regimes is provided. Several distributions with practical importance are considered for the heat-production rate in the numerical examples.

INTRODUCTION

LOCAL heating may be induced by an external heat source (such as a high-intensity laser beam) or may occur as a consequence of deformation. In the former category, both the intensity of the heat source and the geometry of the heating zone can be controlled through the heating devices. This information can thus be used as an input to the energy equation for the determination of the temperature field around the heat source. Typical examples in this category include the short-pulse laser heating on metals [1] and the variation of laser intensity in energy-absorbing materials [2]. The latter category, on the other hand, is a combined effect of thermal and mechanical interactions. Typical examples are local heating in the vicinity of a rapidly propagating crack tip [3–6], temperature rise induced by shear banding [7] and localization of temperature in high-speed penetration [8]. Dissipation of plastic energy is the major heat source in this type of problem which depends on the way in which plasticity is developed in the solid medium. As shown by Taylor and Quinney [9] and Beaver *et al.* [10], more than 90% of the plastic energy dissipates into the form of heat which may induce an extremely high temperature in the local area. For a crack-tip propagating at a speed of 900 m s^{-1} in 4340 steel, as an example, the crack-tip temperature may reach as high as 450°C [11]. In addition to plasticity, friction between a penetrator and a target material is another important heat source in high-speed penetration. For tungsten steel penetrating into aluminum-6061 target, melting may occur in the material layer adjacent to the penetrator which ranges from nanometers to microns depending on the striking velocity. The dynamic coefficient of friction in relation to the frictional heating is still an ongoing research area in this type of problem.

For slower processes such as conventional heat treatment to enhance the local hardness of materials, the classical diffusion model assuming an instantaneous equilibrium may be sufficient to determine the temperature distribution in the work-piece. For the fast process of local heating described in the previous paragraph, however, the process may involve a large heat-flux deposited onto a small area in a short period of time. Metal heating employing a short-pulse laser [1], as an example in the first category, involves a duration of picoseconds which is comparable to the thermal relaxation time of phonons. Local heating in dynamic crack propagation, an example in the second category, occurs in milli- to micro-second range which depends on the crack speed. In addition, the characteristic dimension of the plastic zone may reduce to the order of nanometers for relatively brittle materials [12, 13]. An equilibrium state is impossible within such a short period of time and the use of diffusion model has been questioned when applied to these situations. Temperature in the microscopic two-step model [1, 14] and the macroscopic thermal wave model [15] has been shown to be nonequilibrium and irreversible in nature. Attempts of applying these models to describe heat conduction in short time transient have been made in recent years and interrelations between the two have been established [16, 17]. Most importantly, heat conduction becomes a wave phenomenon when nonequilibrium and irreversible thermodynamic transitions are taken into account [14, 16]. Detailed surveys for research on the two-step model [1] and the thermal wave model [16, 18, 19] have been made extensively and will not be repeated here.

The heating zone involves a finite dimension in most engineering problems. The present study integrates the Green's function of the thermal wave theory [20, 21] to account for the geometrical effect. A heating

NOMENCLATURE

A	area [m^2]
c	parameter, $v/2\alpha$ [m^{-1}]
C	thermal wave speed [m s^{-1}]
C_p	heat capacity [kJ kg^{-1} °C^{-1}]
F, G	combined functions [dimensionless]
k	thermal conductivity [W m^{-1} °C^{-1}]
K_i	modified Bessel function of the second kind of order i, $i = 0, 1$
M	thermal Mach number [dimensionless]
q	volumetric heat generation rate [W m^{-3}]
Q	heat source density per unit length [W m^{-1}]
r	distance in the hypo-space [m]
R	distance between the differential heat source and the observation point in the hypo-space [m]
R^*	dimensionless R
r_0	radius of the circular heating zone [m]
s	dimensionless radial distance centered at the origin of the heat source
t	physical time [s]
T	temperature [°C]
v	speed of the moving heat source [m s^{-1}]
x_i	$i = 1, 2$. Physical coordinates centered at the origin of the heat source [m].

Greek symbols

α	thermal diffusivity [m^2 s^{-1}]
γ	polar angle centered at the observation point [rad]
δ	dimensionless distance
ζ	dimensionless radial distance centered at the observation point
η	radial distance measured from the center of the heat source [m]
θ	polar angle measured from the trailing edge of the heat source [rad]
θ_M	thermal shock angle, $\sin^{-1}(1/M)$ [rad]
ξ_i	$i = 1, 2$. Dimensionless coordinates centered at the origin of the heat source
ρ	mass density [kg m^{-3}]
ϕ	polar angle centered at the origin of the heat source [rad].

Subscripts

$(\ )_{,i}$	$i = 1, 2$. Differentiations with respect to x_i.

zone with a circular shape shall be used to illustrate the procedure. Nonhomogeneous heat intensity generated from the heating zone include the Gaussian distributions for modelling laser irradiations, $1/r$- and $1/\sqrt{r}$-type of distributions for modelling the plastic energy dissipation from a rapidly propagating crack tip.

GREEN'S FUNCTIONS

The thermal Mach number M was introduced by Tzou [20, 21] to characterize the thermal field around a moving heat source. Mathematically, $M = v/C$ with v being the speed of a moving heat source and C the finite speed of heat propagation. The Green's function governing the thermal waves emanating from a *point* heat source satisfies

$$(1-M^2)T_{,11}+T_{,22}+2cT_{,1} = -\frac{Q}{k}\left[\delta(x_1)\delta(x_2)-\left(\frac{M^2}{2c}\right)\delta_{,1}(x_1)\delta(x_2)\right] \quad (1)$$

where (x_1, x_2) are the material coordinates convecting with the point heat source and c a parameter defined as $c = v/2\alpha$. The subscripts in this work, as usual, denote differentiations with respect to space. The mathematical type of equation (1) is depicted by the discriminant $4(M^2-1)$. In the subsonic region with $M < 1$, the equation is elliptic. In transition to the transonic ($M = 1$) and supersonic ($M > 1$) regimes, respectively, the equation transits to a parabolic and a hyperbolic type. Thermal shock waves and thermally undisturbed zones are formed when $M \geqslant 1$. In addition, the finite wave speed induces an apparent heat source term, the derivative of $\delta(x_1)$ with respect to x_1, results from the finite wave speed. The wave amplitude of temperature depicted by equation (1), therefore, is a combined effect of the real heat source exerted on the body and the apparent heat source depending on the *gradient* of the real heat source in the material coordinate system.

Due to intrinsic transition of the mathematical type, the Green's functions satisfying equation (1) were obtained by Tzou [20, 21] in the respective regime of the thermal Mach number. In summary, they are

In the subsonic regime with $M < 1$

$$T(x_1,x_2) = \frac{Q}{k}\exp[-cx_1/(1-M^2)] \cdot\left\{\frac{2-M^2}{2(1-M^2)}K_0\left[\frac{cr}{\sqrt{(1-M^2)}}\right] - \frac{M^2}{2(1-M^2)}K_1\left[\frac{cr}{\sqrt{(1-M^2)}}\right]\right\}. \quad (2)$$

At the transonic stage with $M = 1$

$$T(x_1, x_2) = \frac{Q}{k}\frac{1}{\sqrt{(8\pi c)}}\exp\left[cx_2^2/(2x_1)\right] \cdot \left\{\frac{1}{\sqrt{(-x_1)}} + \frac{cx_2^2 + x_1}{4c\sqrt{(-x_1)^5}}\right\}. \quad (3)$$

In the supersonic regime with $M > 1$

$$T(x_1, x_2) = -\frac{Q}{k}\exp\left[cx_1/(M^2-1)\right] \cdot \left\{\frac{2-M^2}{2(M^2-1)}K_0\left[\frac{cr}{\sqrt{(M^2-1)}}\right] - \frac{M^2}{2(M^2-1)}K_1\left[\frac{cr}{\sqrt{(M^2-1)}}\right]\right\}, \quad (4)$$

with k being the thermal conductivity defined as $\rho\alpha C_p$, Q the heat generation rate per unit length, and K_n the modified Bessel functions of the second kind of order n. The quantity r in equations (2) and (4) is the distance in the hypo-space stretched from the real physical space (x_1, x_2) according to

$$r = \sqrt{\left(\frac{x_1^2}{1-M^2} + x_2^2\right)} \quad \text{for} \quad M < 1$$

$$\text{and} \quad r = \sqrt{\left(\frac{x_1^2}{M^2-1} - x_2^2\right)} \quad \text{for} \quad M > 1. \quad (5)$$

In the subsonic regime with $M < 1$, r is well-defined everywhere in the physical domain and the temperature distribution is represented by equation (2). It reduces to the Green's function for the diffusion equation when M is substituted by zero. In the supersonic regime with $M > 1$, on the other hand, the condition

$$\frac{x_1^2}{M^2-1} > x_2^2 \quad \text{or} \quad |\theta| < \sin^{-1}\left(\frac{1}{M}\right) = \theta_M \quad (6)$$

with θ measured from the *trailing* edge of the heat source shown in Fig. 1(a), must be satisfied to guarantee a real value of r. Equation (6) thus defines the physical domain of the *heat affected zone* in which temperature distribution is represented by equation (4). The rest of the physical domain is defined as the *thermally undisturbed zone* where temperature remains at the reference level due to the finite speed of heat propagation. These situations are illustrated in Fig. 1(c). When the value of M approaches one, i.e. the heat source propagates at the same speed as the thermal wave speed and $M = 1$, the θ-value in equation (6) approaches 90 degrees and the heat affected zone is confined to the domain of $x_1 < 0$ as illustrated in Fig. 1(b). The temperature distribution is represented by equation (5) in this case. When $M \geqslant 1$, most importantly, a strong singularity exists at the thermal *shock* surface at $\theta = \sin^{-1}(1/M)$. The singularity, referring to equation (4), switches from a $\ln(r)$-type (the diffusion theory with $M = 0$) to a $1/r$-type (the wave theory) due to the effect of finite wave speed. Qualitatively, the angle θ_M in equation (6) reveals the *preferential* direction for the accumulation of thermal energy around a fast-moving heat source when the transient time is short [18, 20, 21].

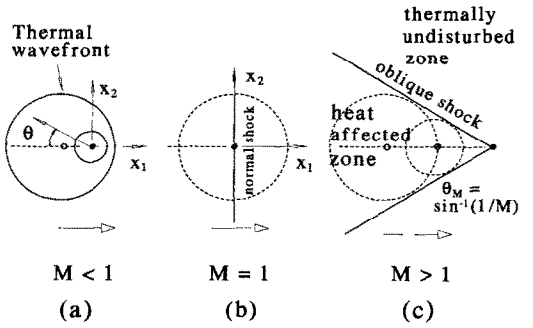

FIG. 1. Configurations and coordinate systems for a point heat source moving in the (a) subsonic, (b) transonic, and (c) supersonic regimes. Angle θ is measured from the trailing edge.

THE CIRCULAR HEATING ZONE

Equations (2)–(4) are the Green's functions which may be integrated for the temperature distributions in a heat-production zone with a finite dimension. For this purpose, the heat-generation rate Q in equations (2)–(4) is replaced by $q\,dA$, with q being the volumetric energy rate deposited into the material volume through the differential surface area dA. Integrations are then performed over the entire physical domain occupied by the heat source. The procedure is straightforward for a heating zone propagating in the subsonic regime where *all* the observation points are located in the heat affected zone. For a heating zone propagating at the transonic and in the supersonic regimes, on the other hand, the integration domains must be carefully examined due to formation of the thermally undisturbed zone. We illustrate this procedure by considering a circular region generating heat with a $1/r$-type of distribution. Here, r denotes the radial distance measured from the center of the heating zone. This type of distribution simulates the thermal energy dissipation due to intensified plasticity developed in the vicinity of a rapidly propagating crack tip [4, 6, 22, 23]. Since the Green's function possesses different expressions in the subsonic, transonic, and the supersonic regimes, the integration must be performed individually.

(a) *The subsonic case with* $M < 1$

Consider a differential heat source $Q = q\,dA$ located at P as shown in Fig. 2. In terms of the polar coordinates (η, ϕ) centered at the origin of the circular region, the temperature can be directly integrated as

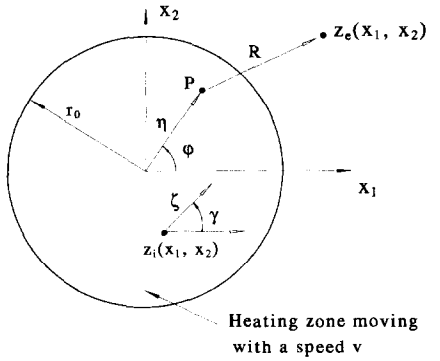

FIG. 2. The central (η, ϕ) and local (ζ, γ) coordinate systems used for describing the temperature distribution around a circular heating zone.

$$T(x_1,x_2)=\frac{q_0}{k}\int_0^{2\pi}\int_0^{r_0}\exp[-c(x_1-\eta\cos\phi)/(1-M^2)]\cdot\left\{\frac{2-M^2}{2(1-M^2)}K_0\left[\frac{cR}{\sqrt{(1-M^2)}}\right]-\frac{M^2}{2(1-M^2)}K_1\left[\frac{cR}{\sqrt{(1-M^2)}}\right]\right\}\times f(x_1-\eta\cos\phi,x_2-\eta\sin\phi)\eta\,d\eta\,d\phi \quad \text{for } M<1 \tag{7}$$

where r_0 is the radius of the circular heating zone, q_0 represents the volumetric energy rate with a distribution described by the function f and

$$R=\sqrt{\left(\frac{(x_1-\eta\cos\phi)^2}{1-M^2}+(x_2-\eta\sin\phi)^2\right)}. \tag{8}$$

A numerical integration is needed for equation (7) due to complexity of the integrand. Introducing the following dimensionless parameters,

$$s=\frac{\eta}{r_0},\quad \xi_1=\frac{x_1}{r_0},\quad \xi_2=\frac{x_2}{r_0}, \tag{9}$$

equation (7) becomes

$$T(\xi_1,\xi_2)=\frac{q_0A}{\pi k}\int_0^{2\pi}\int_0^{1}\exp[-cr_0(\xi_1-s\cos\phi)/(1-M^2)]\cdot\left\{\frac{2-M^2}{2(1-M^2)}K_0\left[\frac{cr_0R^*}{\sqrt{(1-M^2)}}\right]-\frac{M^2}{2(1-M^2)}K_1\left[\frac{cr_0R^*}{\sqrt{(1-M^2)}}\right]\right\}\times f(\xi_1-s\cos\phi,\xi_2-s\sin\phi)s\,ds\,d\phi \quad \text{for } M<1 \tag{10}$$

with

$$R^*=\sqrt{\left(\frac{(\xi_1-s\cos\phi)^2}{1-M^2}+(\xi_2-s\sin\phi)^2\right)} \tag{11}$$

and $A=\pi r_0^2$, the area of the circular zone. For temperature outside the heating zone, z_e in Fig. 2, the regular Gaussian quadrature formula can be applied for the numerical integration of s. For the observation points inside the heating zone, z_i in Fig. 2, a special treatment is needed since equation (10) contains a singularity at $R^*=0$. It occurs when the observation point coincides with the differential heat source, $\xi_1=s\cos\phi$ and $\xi_2=s\sin\phi$. In this case the numerical integration is performed by employing the local coordinates (ζ,γ). In relation to the central coordinates (s,ϕ),

$$s=\sqrt{((\zeta\cos\gamma+\xi_1)^2+(\zeta\sin\gamma+\xi_2)^2)},$$

$$\tan\phi=\frac{\zeta\sin\gamma+\xi_2}{\zeta\cos\gamma+\xi_1}. \tag{12}$$

The integrand of equation (10) can be expressed in terms of ζ and γ according to (12) and the domains of integrations are changed to

$$0\leqslant\gamma\leqslant2\pi \quad \text{and}$$

$$0\leqslant\zeta\leqslant\sqrt{(1+\xi_1\xi_2\sin2\gamma-(\xi_1\sin\gamma)^2-(\xi_2\cos\gamma)^2)}-(\xi_1\cos\gamma+\xi_2\sin\gamma). \tag{13}$$

This procedure reduces the singular part of the integration with respect to ζ (originally s) to the logarithmic type

$$\int_0^1\ln\left(\frac{1}{\zeta}\right)g(\zeta)\,d\zeta \tag{14}$$

with $g(\zeta)$ being a bounded function at $\zeta=0$. The logarithmic Gaussian quadrature formula is then readily applicable for this type of numerical integration [24].

(b) *The supersonic case with* $M>1$

In a similar fashion of obtaining equation (10) from equation (2), equation (4) is used instead in this case for the temperature distribution. Formation of the thermally undisturbed zone when $M\geqslant1$ constitutes additional difficulty in determining the domains of integrations. For the circular region moving at a certain thermal Mach number M (and hence every differential heat source inside), as shown in Fig. 3, the field point P may be located in the heat affected zone of S_1 and in the thermally undisturbed zone of S_2. The Green's function for the heat affected zone is

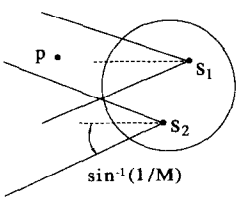

FIG. 3. Location of the observation point P inside the heat affected zone of the differential heat source S_1 and the thermally undisturbed zone of S_2. The wedge angle is $2\sin^{-1}(1/M)$ for the heat affected zone.

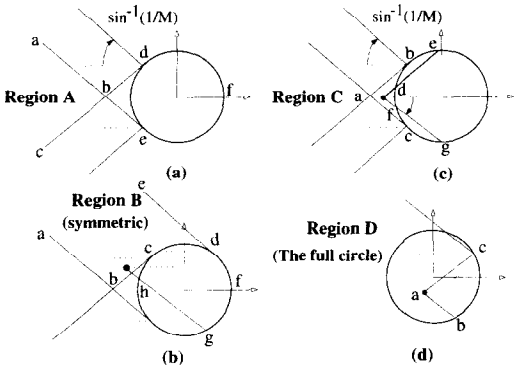

FIG. 4. Regions A, B, C and D and their corresponding domains of integrations in the circular heating zone. Supersonic regime with $M > 1$.

represented by equation (4) while remaining at zero in the thermally undisturbed zone due to the finite speed of heat propagation. The physical domain containing S_2, therefore, has to be excluded in the numerical integration for temperature at P.

Figures 4(a)–(d) summarize the four regions, A–D, in the wake area of the heating zone under such considerations. Region A shown in Fig. 4(a) is represented by the wedge area *abc* extending to infinity. Mathematically,

$$\xi_1 \leqslant -\frac{1}{\sin\theta_M},$$

$$0 \leqslant \xi_2 \leqslant -\cos\theta_M - (\xi_1 + \sin\theta_M)\tan\theta_M \quad \text{for region A} \qquad (15)$$

where only the expression in the upper-half plane is given due to symmetry. The field point in region A is located in the heat affected zone emanating from any differential heat source inside the circular region represented by *defd* in Fig. 4(a). The integration domain is thus $s \in [0, 1]$ and $\phi \in [0, 2\pi]$, the entire circular region. Region B is represented by the area *abcde* in Fig. 4(b). Mathematically,

$$-\theta_M \leqslant \gamma \leqslant \cos^{-1}\frac{\xi_2 - \xi_1\sqrt{(\xi_1^2+\xi_2^2-1)}}{\xi_1^2+\xi_2^2},$$

$$F \leqslant \zeta \leqslant G \quad \text{for region B} \qquad (16)$$

with

$$F = -(\xi_1\cos\gamma + \xi_2\sin\gamma) - \sqrt{(1+\xi_1\xi_2\sin 2\gamma - \xi_1^2\sin^2\gamma - \xi_2^2\cos^2\gamma)}$$

$$G = -(\xi_1\cos\gamma + \xi_2\sin\gamma) + \sqrt{(1+\xi_1\xi_2\sin 2\gamma - \xi_1^2\sin^2\gamma - \xi_2^2\cos^2\gamma)}. \qquad (17)$$

This region is located in the heat affected zone for any differential heat source within the circular sector *hcdfgh*. Unlike region A, however, segment *cd* in this case is in contact with the heat-generation zone. Singularities thus result in the numerical integrations and local coordinates (ζ, γ) are used instead in equation (16) for a logarithmic-type of integral (refer to equation (14)). Region C is represented by the closed area *abdfca* in Fig. 4(c). The differential heat sources contributed to the temperature level within region C are located in the area *edfge* within the circular area. This area also contacts with the heat-generation zone and the domains of integration are

$$-\theta_M \leqslant \gamma \leqslant \theta_M, \quad F \leqslant \zeta \leqslant G. \qquad (18)$$

Region D, lastly, is the entire physical domain within the heat-generation zone. Any point inside the circular region is located in the heat affected zones emanating from the differential heat sources at c and b and the integration domain is thus the area represented by *abc* in Fig. 4(d):

$$-\theta_M \leqslant \gamma \leqslant \theta_M, \quad 0 \leqslant \zeta \leqslant G. \qquad (19)$$

In evaluating the temperature at a certain point in the physical domain, therefore, it is necessary to identify the region in which the point belongs to. Appropriate integration domains are then selected from equations (16)–(19) in numerical integrations.

(c) *The transonic stage with* $M = 1$

At $M = 1$, as shown in Fig. 1(b), a normal shock wave exists at $\xi_1 = 0$ (coincident with the ξ_2 axis) and the heat affected zone is in the region with $\xi_1 < 0$. Equation (3) is used in this case for the temperature distribution. Two regions, A and B summarized in Fig. 5, exist in this case. Region A is the entire area behind the circular heating zone ($\xi_1 < -1$) and the domains of integration are $s \in [0, 1]$ and $\phi \in [0, 2\pi]$ covering the entire circle. Region B is the physical domain of the strip represented by $-1 < \xi_1 < 1$. The temperature level at a material point located at ξ_1 (represented by *ab* in Fig. 5) is contributed by all the differential heat sources within the area of *abca*. Only the differential heat sources in the shaded area contribute to its temperature rise. The domain of integration is thus from ξ_1 to 1 within the circular area. Similar to the previous cases in Figs. 4(b)–(d), region B is in contact with the heat-generation zone and singularities thus result in the numerical integrations. Unlike the previous cases with a $\ln(r)$-type of singularity, however, the singularity in this case is unremovable and an asymptotic algorithm is used. The

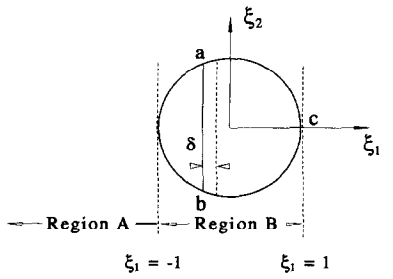

FIG. 5. Regions A ($\xi_1 < -1$) and B ($-1 < \xi_1 < 1$) at the transonic stage with $M = 1$ and the deviation δ from a representative location of ξ_1.

location of ξ_1 is deviated to $\xi_1-\delta$, refer to Fig. 5, in the numerical integration from ξ_1 to 1. Convergence of the temperature distribution is then studied when δ approaches zero.

NUMERICAL EXAMPLES

The numerical algorithms thus developed are first validated by comparing to the solutions of diffusion obtained by Weichert and Schönert [12]. For a circular heating zone propagating at speeds of 200 and 1000 m s^{-1}, the diffusion model was employed to determine the temperature distributions. Their results are retrieved in equation (10) by substituting M by zero since the thermal wave speed is assumed infinity ($C\to\infty$) in diffusion. The following parameters

$$r_0 = 3\times10^{-9}\ \text{m},\quad k = 1\ \text{W m}^{-1}\ \text{K}^{-1},$$
$$\alpha = 5\times10^{-7}\ \text{m}^2\ \text{s}^{-1} \tag{20}$$

are used in their analysis. The heat intensity is assumed to be constant, $q_0 = 5\times10^{18}\ \text{W m}^{-3}$. For $v = 200$ and 1000 m s^{-1} and $M = 0$, Fig. 6 shows the temperature contours obtained by the present algorithm (the full circles) and those by Weichert and Schönert [12] (the solid lines). The dashed circle represent the physical domain of the heating zone which, according to equation (9), has been normalized to $\xi_1\in[-1,1]$ and $\xi_2\in[-1,1]$. The numerical integration employs the ten-point Gaussian quadrature formula which yields an excellent agreement.

The thermal wave speed C plays a dominant role in the wave theory of heat conduction. Due to absence of this information for glass, we consider the material properties of 4340 steel with the following properties:

$$r_0 = 4\times10^{-8}\ \text{m},\quad k = 34\ \text{W m}^{-1}\ \text{K}^{-1},$$
$$\alpha = 1.0\times10^{-5}\ \text{m}^2\ \text{s}^{-1},\quad q_0 = 5\times10^{18}\ \text{W m}^{-3},$$
$$C = 900\ \text{m s}^{-1}. \tag{21}$$

The value of C (900 m s^{-1} for the thermal wave speed) is assumed here due to several unique features preserved in the transonic solution when compared to the experimental results [25], which also supports the use of the wave-type equation (1) for the present problem. In the sequel dimensionless temperature defined as $T/(qA/k)$ will be used in presenting the temperature surfaces.

(a) *Gaussian distributions*

The distribution function f is needed in equation (10) for numerical integrations. The Guassian distribution

$$f(x,y) = e^{-5(x^2+y^2)} \tag{22}$$

is first considered to model a moving laser source impinged upon the surface of a work-piece. The parameter five (5) in equation (22) is actually the reciprocal of the square of the characteristic radius of a laser beam. This is the radius within which 63% of the incident energy lies. Figure 7 presents the temperature surfaces in transition of the thermal Mach number. The circular heating zone occupies the physical domain for $\xi_1\in[-1,1]$ and $\xi_2\in[-1,1]$. Due to the symmetry of the problem, however, only the results in the upper-half plane with $\xi_2\in[0,1]$ are presented. In the subsonic regime shown by Figs. 7(a) and (b), the temperature level decreases when the thermal Mach number increases. In transition to the transonic stage shown by Fig. 7(c), the temperature level continuously decreases while the temperature surface warps around the edge due to formation of the normal shock surface. In comparison with the case of a point heat source [1, 2], temperature drop across the shock surface is much weaker. The corresponding case of diffusion with $v = 900$ m s^{-1} and $M = 0$ is shown in Fig. 7(d) for comparisons. The temperature level predicted by the wave theory is about one order of magnitude *lower*. The temperature surfaces in the supersonic regime are shown in Figs. 7(e) and (f). The temperature level slightly increases with the thermal Mach

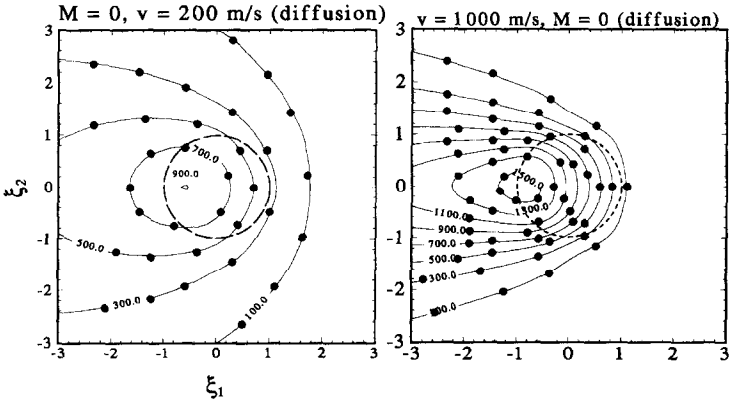

FIG. 6. Comparisons with the results of diffusion obtained by Weichert and Schönert [12]. Full circles—present analysis. Solid line—Weichert and Schönerts' results. $M = 0$ and (a) $v = 200$ m s^{-1} and (b) $v = 1000$ m s^{-1}.

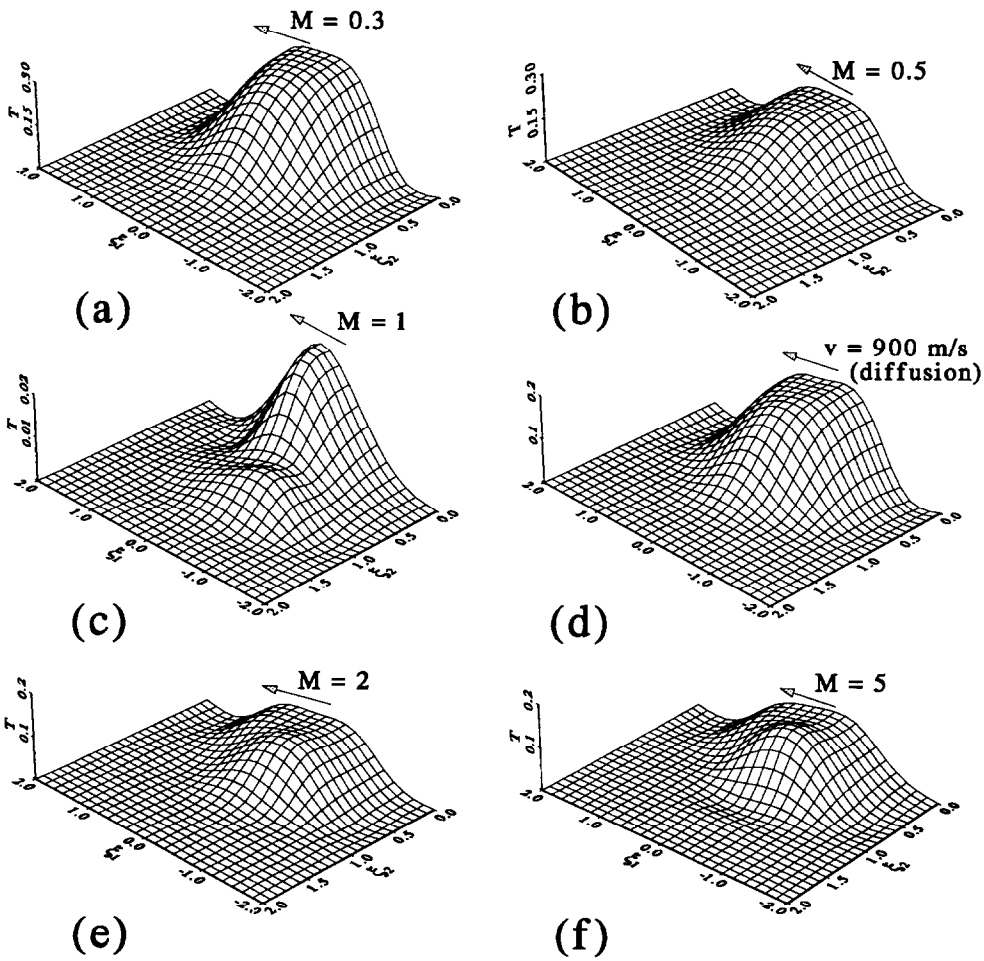

FIG. 7. Evolution of temperature waves from subsonic ((a) and (b)), transonic ((c)), to supersonic ((e) and (f)) regimes. Heat intensity with a Gaussian distribution.

number but is relatively minor in comparison with the case with a point heat source. Dimples in the temperature surfaces, refer to Figs. 7(c), (e) and (f), are the combined results of the distribution function of the heat intensity and the formation of thermal shock surfaces (though weak in the present problem). For a circular heating zone propagating to the front, the high-temperature region shifts toward the rear end. While the thermal energy in the high-temperature region is dissipating into the surrounding media, it is also confined by the thermal shock surface due to formation of the thermally undisturbed zone. Dimples in the temperature surfaces reflect the way in which the high-temperature reduces to the room temperature (assumed zero in this work) across the thermal shock surfaces.

(b) $1/r$-*type distributions*

In dynamic crack propagation, heat is generated at the crack tip due to intensified, high-rate plasticity induced by the crack speed. The localized heating zone is convecting with the crack tip in the history of propagation and the problem can be modelled by the one with a moving heat source [3–6, 12, 13]. The heat intensity in this case, unlike the externally controlled heating, is dictated by the stress and the plastic-strain-rate distributions developed in the vicinity of the crack tip. The product of the stress and the plastic strain rate tensors gives the dissipation rate of plastic energy which is converted to heat in crack propagation. Distribution of thermal energy in the heating zone depends on the material type and is a weak function of the crack speed in the practical range. The $1/r$-type distribution, with r being the distance measured from the moving crack tip, covers a wide range of engineering materials (such as metals) with a relatively brittle behavior. The distribution function in equation (22) is replaced by

$$f(x, y) = \frac{1}{\sqrt{(x^2+y^2)}} \tag{23}$$

in this case and equation (23) is employed in the numerical integrations of equation (10). The results

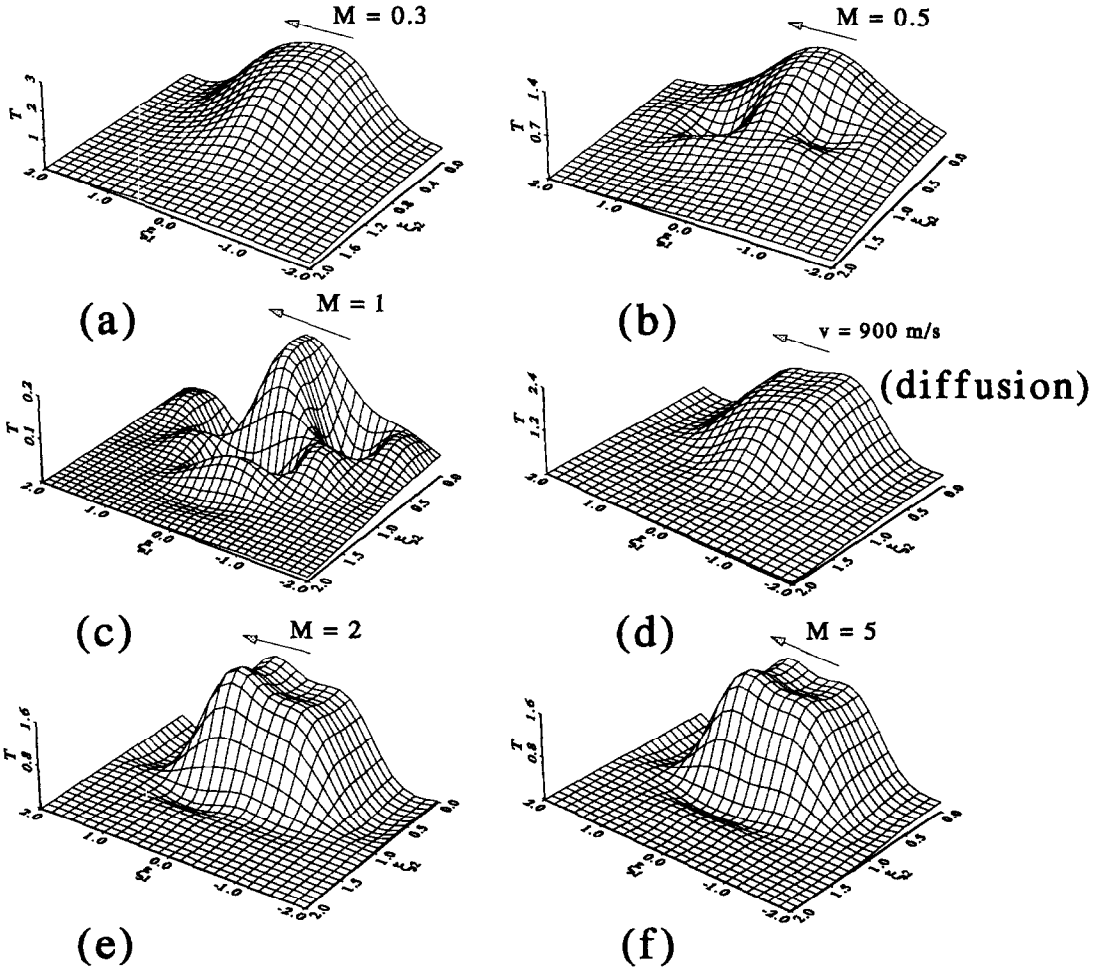

FIG. 8. Evolution of temperature waves from subsonic ((a) and (b)), transonic ((c)), to supersonic ((e) and (f)) regimes. Heat intensity with a $1/r$-type distribution.

covering the entire regimes of the thermal Mach number are shown in Fig. 8. Due to the singular behavior in the distribution near the center at $r = 0$, as shown by Fig. 8(b), the temperature surface starts to distort at $M = 0.5$. Formation of the normal shock waves at $M = 1$, as shown in Fig. 8(c), promotes the distortion which presents a different situation from that in the previous case without a singularity. Comparing Figs. 8(c) and (d) for the corresponding diffusion behavior, more significant differences result. The wave theory, however, still predicts a lower temperature level in comparison with diffusion. The cases in the supersonic regime with $M = 2$ and 5, respectively, are shown in Figs. 8(e) and (f). To be noticed is that the angular distribution of heat intensity is still not modelled in this example. Reflected by equation (23), the heat intensity has the same value for material points at the same distance from the center of the heating zone. For real problems in dynamic crack propagation, therefore, the angular distribution should be addressed in equation (23) for a closer simulation.

(c) $1/\sqrt{r}$-*type distributions*

Some viscoplastic materials present a bounded plastic strain rate at the dynamically propagating crack tip while the stress field still possesses a $1/\sqrt{r}$-type of singularity [5, 26]. The plastic energy dissipation rate, and hence the thermal energy dissipation rate, consequently displays a $1/\sqrt{r}$-type of singularity at the crack tip. For the sake of completeness, the results for this case are also obtained and shown in Fig. 9. The distribution function in this case is replaced by

$$f(x, y) = \frac{1}{(x^2 + y^2)^{1/4}} \tag{24}$$

in integrating equation (10). From a mathematical point of view, the $1\sqrt{r}$-type distribution shown by (24) is less singular than the $1/r$-type distribution shown by (23). The warping behavior of the temperature surface, therefore, is between case (a) (Fig. 7) and (b) (Fig. 8). Similar behavior of the temperature surfaces are observed in transition of the thermal Mach number.

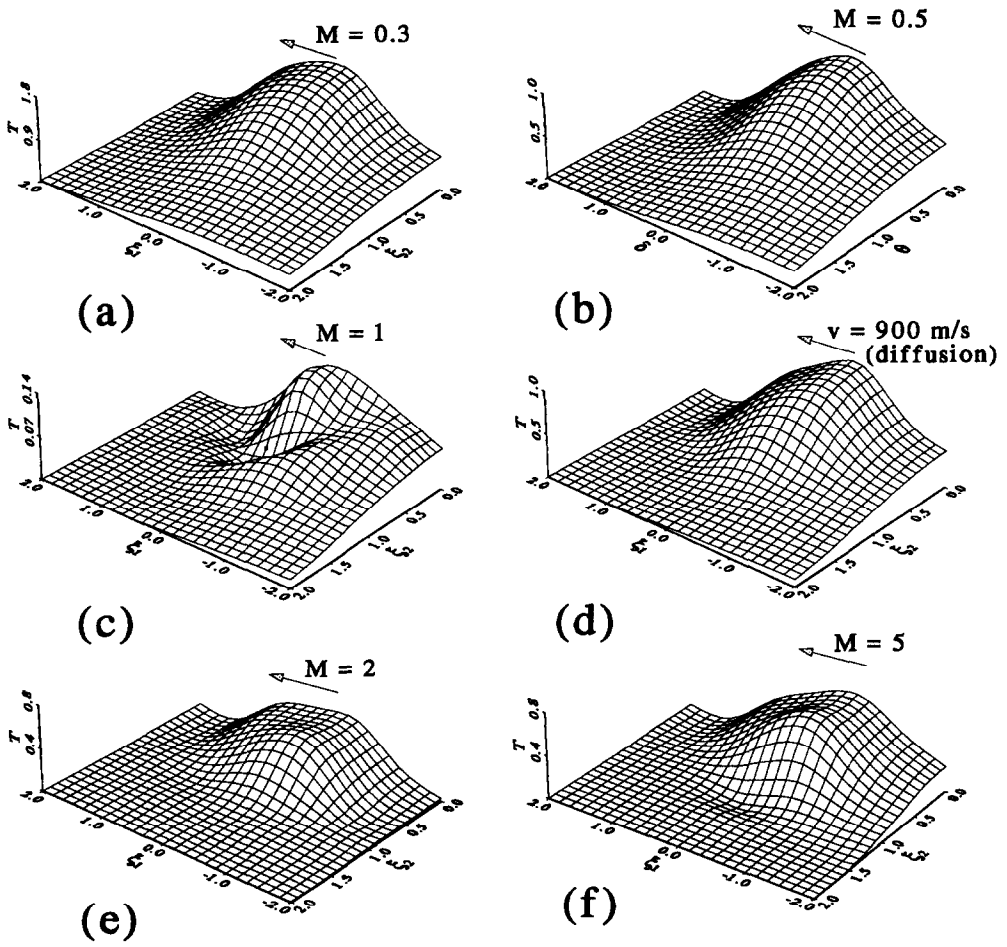

FIG. 9. Evolution of temperature waves from subsonic ((a) and (b)), transonic ((c)), to supersonic ((e) and (f)) regimes. Heat intensity with a $1/\sqrt{r}$-type distribution.

In comparison with diffusion, refer to Figs. 7(d), 8(d) and 9(d), we note that the temperature surfaces employing the wave theory are more oscillatory especially at the transonic and in the supersonic regimes. It directly implies a more pronounced wave behavior when the heating zone propagates at a higher speed [27].

CONCLUSION

The temperature distribution around a fast-moving heat source with a finite dimension has been obtained by integrating the Green's functions in the thermal wave theory. The procedure is illustrated by a heating zone with a circular geometry. Formation of the thermally undisturbed zone at the transonic stage and in the supersonic regime constitutes a complicated situation in numerical integrations for temperature. Unlike the diffusion theory where integrations are simply performed over the entire area of the heating zone, the heating zone has to be divided into several areas according to the location of the observation point. Regions A to B and the corresponding domains of integrations summarized in Fig. 4 illustrate this situation in terms of a heating zone with a circular shape. Should the geometry of the heating zone vary, these domains must be adjusted accordingly while the rest of the procedure in numerical integrations remain the same. Currently, the procedure has been successfully applied to the case with a rectangular heating zone and extension to the high-rate zone with a butterfly shape existing in real problems of dynamic crack propagation is on the way.

The present analysis is sufficient for externally controlled heatings with distributions and geometries known a priori. For modelling real problems in dynamic crack propagation, however, it also relies on a detailed description of the stress and strain fields in the near-tip region. In addition to the effort devoted to the geometry of the localized heating zone, the phonon-drag controlled process in high-rate plasticity [28] is currently implemented into the analysis to describe the heat-production rate. While the strain-rate effect is accommodated in describing the material

behavior in the near-tip region, we believe that the thermal wave theory accounting for the high-rate response in heat conduction is more consistent in describing the local heating phenomenon. Lastly, all the thermal properties have been assumed constant in this analysis. When the thermal conductivity becomes strongly dependent on the temperature gradient, equation (1) becomes nonlinear and a major modification must be made to the current solutions to accommodate such an effect.

Acknowledgement—The work is accomplished in the course of research supported by the Mechanics and Materials Program at the National Science Foundation under Grant No. MSS-9200993 with the University of New Mexico.

REFERENCES

1. T. Q. Qiu and C. L. Tien, Short-pulse laser heating on metals, *Int. J. Heat Mass Transfer* **35,** 719–726 (1992).
2. B. F. Blackwell, Temperature profile in semi-infinite body with exponential source and convective boundary condition, *ASME J. Heat Transfer* **112,** 567–571 (1990).
3. J. R. Rice and N. Levy, Local heating by plastic deformation at a crack tip. In *The Physics of Strength and Plasticity* (Edited by A. S. Argon). MIT Press, Cambridge (1969).
4. Z.-B. Kuang and S. Atluri, Temperature field due to a moving heat source: a moving mesh finite element analysis, *ASME J. Appl. Mech.* **52,** 274–280 (1985).
5. J. C. Sung and J. D. Achenbach, Temperature at a propagating crack tip in a viscoplastic material, *J. Thermal Stresses* **10,** 243–262 (1987).
6. A. S. Douglas and H. U. Mair, The temperature field surrounding a dynamically propagating mode III crack, *Scripta Metallurgia* **21,** 479–484 (1987).
7. K. A. Hartley, J. Duffy and R. H. Hawley, Measurement of the temperature profile during shear band formation in steels deforming at high strain rates, *J. Mech. Phys. Solids* **35,** 283–301 (1987).
8. D. Y. Tzou, M. J. Forrestal and L. B. Longcope, Dynamic spherical cavity-expansion for Mohr–Coulomb materials with a tension cutoff, *Int. J. Impact Engng* (submitted for publication).
9. G. I. Taylor and M. A. Quinney, The latent heat remaining in a metal after cold work, *Proc. Roy. Soc. (A)* **143,** 307–326 (1974).
10. M. B. Bever, D. L. Holt and A. L. Titchener, The stored energy of cold work, *Proc. Mat. Sci.* **17,** 354–377 (1973).
11. A. T. Zehnder and A. J. Rosakis, On the temperature distribution at the vicinity of dynamically propagating cracks in 4340 steel, *J. Mech. Phys. Solids* **39,** 385–415 (1991).
12. R. Weichert and K. Schönert, On the temperature rise at the tip of a fast running crack, *J. Mech. Phys. Solids* **22,** 127–133 (1974).
13. R. Weichert, Heat generation at the tip of a moving crack, *J. Mech. Phys. Solids* **26,** 151–161 (1978).
14. D. Y. Tzou, R. Chiffelle and M. N. Özisik, On the rate effect in nonequilibrium temperature waves, *ASME J. Heat Transfer* (in press).
15. D. Y. Tzou, An engineering assessment to the relaxation time in the thermal wave theory, *Int. J. Heat Mass Transfer* **36,** 1845–1851 (1993).
16. M. N. Özisik and D. Y. Tzou, On the wave theory in heat conduction, *Session on Significant Questions: Fundamental Issues in Microscale Heat Transfer*, 1992 ASME Winter Annual Meeting, Anaheim, California (1992).
17. D. Y. Tzou and M. N. Özisik, Interrelations between the microscopic two-step model and the macroscopic thermal wave model, *ASME J. Heat Transfer* (in press).
18. D. Y. Tzou, Thermal shock phenomena in solids under high rate response. In *Annual Review of Heat Transfer* (Edited by C. L. Tien), Chap. 3. Hemisphere, Washington, D.C. (1992).
19. D. D. Joseph and L. Preziosi, Heat waves, *Rev. Modern Phys.* **61,** 41–73 (1989).
20. D. T. Tzou, On the thermal shock wave induced by a moving heat source, *ASME J. Heat Transfer* **111,** 232–238 (1989).
21. D. Y. Tzou, Shock wave formation around a moving heat source in a solid with finite speed of heat propagation, *Int. J. Heat Mass Transfer* **32,** 1979–1987 (1989).
22. D. Y. Tzou, Thermal shock waves induced by a moving crack, *ASME J. Heat Transfer* **112,** 21–27 (1990).
23. D. Y. Tzou, Thermal shock waves induced by a moving crack—a heat flux formulation, *Int. J. Heat Mass Transfer* **33,** 877–885 (1990).
24. A. H. Stroud and P. Secrest, *Gaussian Quadrature Formula*. Prentice-Hall, New Jersey (1966).
25. D. Y. Tzou, The thermal shock phenomena induced by a rapidly propagating crack tip: experimental evidence, *Int. J. Heat Mass Transfer* **35,** 2347–2356 (1992).
26. S. R. Bonder and Y. Partom, Constitutive equations for elastic-viscoplastic strain-hardening materials, *ASME J. Appl. Mech.* **42,** 385–389 (1975).
27. D. Y. Tzou, Thermal resonance under frequence excitations, *ASME J. Heat Transfer* **114,** 310–316 (1992).
28. L. B. Freund and J. W. Hutchinson, High strain-rate crack growth in rate-dependent plastic solids, *J. Mech. Phys. Solids* **33,** 169–191 (1985).